METALLURGY

Multiplicity of dislocation pathways in a refractory multiprincipal element alloy

Fulin Wang[1], Glenn H. Balbus[1], Shuozhi Xu[2], Yanqing Su[3], Jungho Shin[1], Paul F. Rottmann[4], Keith E. Knipling[5], Jean-Charles Stinville[1], Leah H. Mills[1], Oleg N. Senkov[6], Irene J. Beyerlein[1,2,3], Tresa M. Pollock[1], Daniel S. Gianola[1]*

Refractory multiprincipal element alloys (MPEAs) are promising materials to meet the demands of aggressive structural applications, yet require fundamentally different avenues for accommodating plastic deformation in the body-centered cubic (bcc) variants of these alloys. We show a desirable combination of homogeneous plastic deformability and strength in the bcc MPEA MoNbTi, enabled by the rugged atomic environment through which dislocations must navigate. Our observations of dislocation motion and atomistic calculations unveil the unexpected dominance of nonscrew character dislocations and numerous slip planes for dislocation glide. This behavior lends credence to theories that explain the exceptional high temperature strength of similar alloys. Our results advance a defect-aware perspective to alloy design strategies for materials capable of performance across the temperature spectrum.

The history of materials advancement over centuries has been anchored by the tenet of utilizing one principal element and adding dilute concentrations of alloying elements to achieve the properties of interest. The past decade has witnessed a shift toward an alloy design strategy focusing on the center of multicomponent compositional space. Termed multiprincipal element alloys (MPEAs), complex concentrated alloys, or most commonly as a subclass of these materials known as high-entropy alloys, some of these materials exhibit exceptional combinations of strength, ductility, and damage tolerance (*1*–*5*). Refractory alloys are attractive candidates for use at extremely high temperatures as is demanded by many technology applications, particularly in the aerospace and power-generation sectors (*6*, *7*). Progress in alloy development in this material class, however, has been slow and stands to benefit from the MPEA design paradigm.

The desire for materials with thermally stable microstructures and temperature-insensitive properties has inspired the development of a family of body-centered cubic (bcc) refractory MPEAs (*7*, *8*). These alloys made up a near equiatomic mixture of refractory metal elements. The high strengths displayed, at high temperatures in particular, are very attractive because they surpass state-of-the-art Ni-based superalloys in some cases, which often lose strength at temperatures above 1200°C (*3*, *7*). Alloys that can remain strong at high temperatures enable increased operating temperatures with improved efficiency in a variety of energy, aerospace, and nuclear applications. Alloys with the bcc crystal structure, including steels, are ubiquitous. These alloys are the foundation of a vast array of structures and technologies because of their economies of scale. However, conventional bcc alloys are plagued by a pronounced dependence of the mechanical properties on temperature, which often manifests as a ductile-to-brittle transition with decreasing temperature. The origin of this behavior is linked to the sluggish motion of screw dislocations, which are linear crystalline defects that allow plastic strain accommodation, owing to the nature of the atomic bonding at the dislocation core, and/or embrittlement by interstitial elements such as C, O and N. Increasing temperature mobilizes screw dislocations (in a catch-up game with their edge dislocation counterparts) to enable noncatastrophic shape changes, albeit at the expense of strength. In contrast to many bcc pure metals and dilute alloys, some bcc refractory MPEAs such as MoNbTaW and MoNbTaVW exhibit a gradual decrease of strength with increasing temperature and even a strength plateau in the intermediate temperature range of 600° to 1000°C (*9*) (Fig. 1).

The high strength of single-phase bcc MPEAs is fundamentally related to (i) solute strengthening by the concentrated compositions and (ii) the variation of core structure along a screw dislocation due to local chemical fluctuations (*10*, *11*). Both phenomena suggest that the thermally activated kink nucleation on a screw dislocation is not necessarily the rate-limiting step for dislocation motion, as it is for simple bcc metals (*12*), leading to the prediction of a weak temperature dependence of strength. However, the diversity of macroscopic behavior of different MPEAs (Fig. 1A) has eluded theoretical interpretations and, thereby, a clear mechanistic picture. Furthermore, unlike their face-centered cubic MPEA counterparts, there is limited experimental evidence of the underlying deformation mechanisms in bcc MPEAs, which thus far does not sufficiently support some analytical models (*11*). For instance, dislocations in the deformed bcc MPEA HfNbTaTiZr were observed to exhibit a strong screw character (*13*), a feature indicating the distinctly easy glide of edge compared with screw dislocations, in accordance with the classical kink mechanism of screw dislocations in bcc metals. The dominance of screw dislocations appears to be incommensurate with theoretical predictions of dislocations in MPEAs, such as preexisting kinks on a tortuous screw dislocation and the retarded motion of nonscrew dislocations. Both predictions would render dislocation lines with appreciable deviations from a pure screw orientation. Taken as a whole, the current picture depicted by experiments suggests that classical bcc dislocation mechanisms (Fig. 1C), with only subtle augmentations, are operative in MPEAs. This would be an unexpected finding, given the ruggedness of the atomic landscape that dislocations must navigate in these alloys (Fig. 1D).

A robust understanding of the mechanistic origin of the distinctive properties in the bcc MPEAs that exhibit weak temperature-dependent behavior would greatly inform alloy design principles. We experimentally demonstrated a striking departure from conventional bcc dislocation behavior in the MPEA MoNbTi, an alloy that shows decent strength at low temperature and an intermediate temperature-strength plateau yet a considerably lower density (ρ = 7.67 g/cm^3) (Fig. 1, A and B) (*14*). Moreover, the combination of these three elements reflects one of the most frequently used base blocks of the reported refractory MPEAs (*7*), among which are the ductile and strong examples of HfMoNbTiZr and MoNbTiV. We focused on elucidating the intrinsic capacity for plastic deformation by dynamically probing dislocations in the single bcc phase and single-crystal environment, at equiatomic composition with global randomness (Fig. 1, E and F). Experiments were performed at room temperature [0.12 melting temperature (T_m)], which is below the classical transition temperature of ~0.2 T_m (*12*, *15*), at which thermally activated kink-pair nucleation ceases to be the rate-limiting step. This temperature enabled us to probe differences in the dislocation slip behavior in MPEAs and conventional bcc metals. Our results highlight multiplanar, multicharacter dislocation slip in MoNbTi, encouraged by the broad dispersion in the glide resistance for dislocations, due to the atomic-scale chemical fluctuations. The ability of

[1]Materials Department, University of California, Santa Barbara, CA, USA. [2]California NanoSystems Institute, University of California, Santa Barbara, CA, USA. [3]Department of Mechanical Engineering, University of California, Santa Barbara, CA, USA. [4]Department of Chemical and Materials Engineering, University of Kentucky, KY, USA. [5]Materials Science and Technology Division, U. S. Naval Research Laboratory, Washington, DC, USA. [6]Air Force Research Laboratory, Wright-Patterson AFB, OH, USA.
*Corresponding author. Email: gianola@ucsb.edu

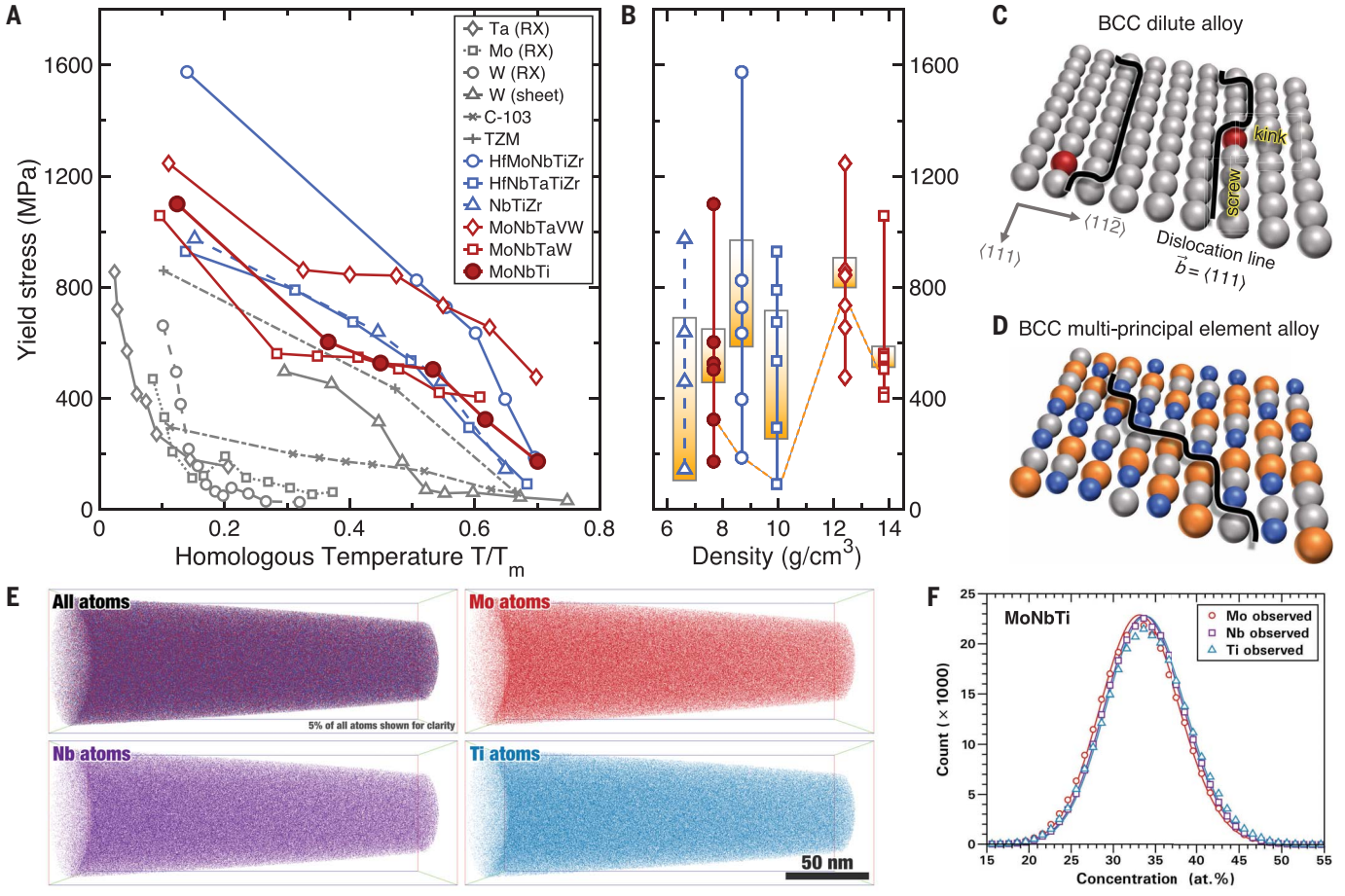

Fig. 1. The temperature dependence of the yield stress of the equiatomic MoNbTi alloy. (**A**) Representative refractory MPEAs are bcc phase polycrystals tested in compression (*22*, *25*). For comparison, the tensile yield stresses of pure bcc metals in either recrystallized (RX) or rolled condition (sheet) are included (*26*, *27*), as are those of the commercial dilute alloys C-103 (a Nb-based alloy) and TZM (a Mo-based alloy, Mo-Ti-Zr) (*28*, *29*). (**B**) Densities are from (*22*). The topmost data are at room temperature. The boxes highlight the yield strengths in the temperature range of 600° to 1000°C. Those at 1200°C are connected by the dashed orange line. (**C** and **D**) Schematic depictions of the dislocation morphologies on the {1$\bar{1}$0} slip plane in bcc dilute alloy and in bcc MPEA, respectively. (**E**) Atom probe tomography reconstructions (87 nm by 87 nm by 246 nm) containing 29.5 × 10^6 identified ions (*14*), showing the spatial distribution of all the atoms and of Mo, Nb, or Ti atoms individually. (**F**) Concentration of alloying elements in this analyzed volume is 33.181 Mo–33.272 Nb–33.188 Ti [atomic % (at.%)], with trace amounts of interstitial N, O, and C. The comparison with a theoretical binomial distribution (solid line) confirms that Mo, Nb, and Ti are homogeneously distributed.

dislocations to choose the easy gliding direction and plane in the random field of multiple atomic species enables an excellent combination of strength and homogeneous plasticity in this alloy, traits that are not simultaneously observed in conventional metallic alloys.

Characterization of dislocations after nanoindentation

We first select the multiaxial stress state imposed during indentation, as it provides an avenue to investigate all potential configurations of dislocations. The microstructure of the as-processed MoNbTi is initially free from dislocations, as demonstrated by the uniform contrast outside the plastic zone created by the indentation (Fig. 2); thus all the dislocations we observed underwent glide to their rest positions. Detailed analyses of the dislocation Burgers vector and line direction were performed in an area containing discernable individual dislocations (tables S2 and S3). We identified two groups of dislocations with the Burgers vectors of 1/2[$\bar{1}$11] and 1/2[11$\bar{1}$], respectively. The segments of the 1/2[$\bar{1}$11] dislocations that lie roughly vertical in the images are close to screw character, whereas the segments that are approximately horizontal are close to edge character. The morphological deviation away from a straight pure screw orientation indicates a substantial tortuosity with segments of nonscrew character along the otherwise rectilinear screw dislocation (fig. S2). Dislocations #2 to #6 are close to pure edge ones and exist on distinct slip planes, including (211), (321), and (110). Dislocations #7 and #8 have one segment of edge or mixed character (roughly horizontal in the images) and the other segment close to screw character (roughly vertical in the images), with both habiting the (110) plane. The dislocations in the second group have a Burgers vector of 1/2[11$\bar{1}$] and are parallel to each other, as represented by dislocation #9 (Fig. 2F). These dislocations appear at an angle to the projection of their Burgers vector 1/2[11$\bar{1}$] at the diffraction condition of $\mathbf{g}_3$ (Fig. 2D), indicating that they are all mixed dislocations. Both the presence of substantial nonscrew segments and high-order slip planes are unexpected for bcc metals at such low homologous temperature (0.12 T_m). Furthermore, dislocations #1 to #8 have the same Burgers vector and are subjected to a similar stress state on the basis of their close proximity to each other, suggesting that the propensity of

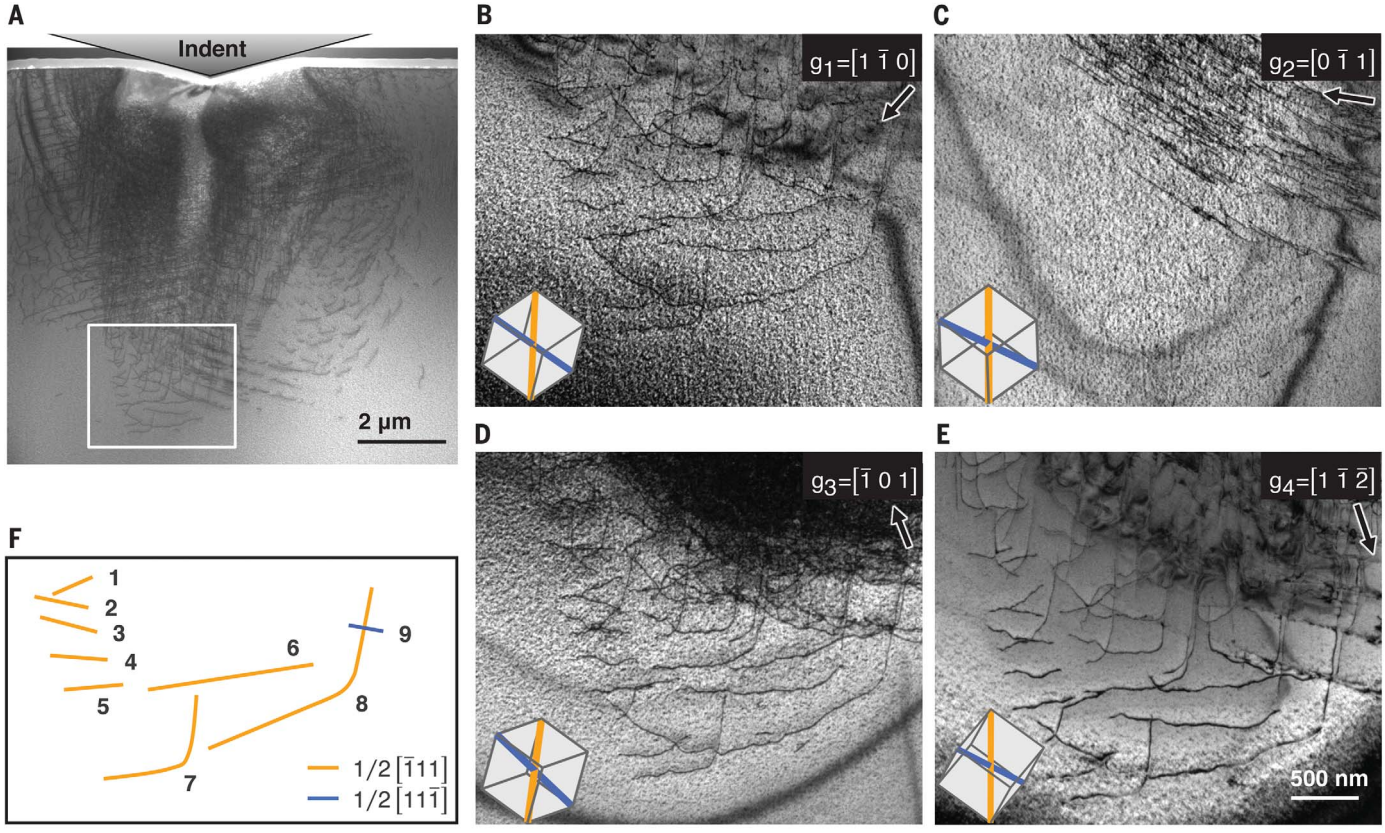

Fig. 2. Dislocations induced by nanoindentation. The scanning transmission electron microscopy (TEM) image in (**A**) shows an overview of the dislocations under the indent. (**B** to **E**) Two-beam bright-field TEM images of the boxed area in (A). The diffraction vector, **g**, is annotated in each image with the direction shown by the arrow. The crystal orientation is indicated with a cubic lattice in the respective image. The Burgers vectors are drawn in the lattices, with the orange line denoting 1/2[$\bar{1}$11] and the blue line denoting 1/2[11$\bar{1}$]. (**F**) shows schematically the dislocations numbered 1 to 9 for dislocation line direction analysis. They are colored according to the respective Burgers vector.

dislocations to glide on various planes may be similar.

Dislocations during single-crystal tensile deformation

We assessed the dynamic behavior of dislocations during plastic deformation using quantitative in situ tensile tests, which revealed cross-slip and bowing of dislocations, providing key insights on the mechanisms mediating dislocation glide. We conducted tensile loading of the single-crystal sample close to the [001] crystal direction, resulting in equal resolved shear stresses (RSSs) along all four possible ⟨111⟩ Burgers vectors. We quantitatively determined the full crystallographic characteristics of the gliding dislocations, including Burgers vector, slip plane, and line direction, with high fidelity (14) and uncovered the substantial nonscrew character of gliding dislocations in MoNbTi (Fig. 3). All of the dislocations shown in Fig. 3 glide along the traces at the same angle of −61° to the tensile direction, corresponding to a distinctive 1/2[$\bar{1}$1$\bar{1}$]($\bar{2}$13) slip system (table S4). We reconstructed the line morphology of dislocation (iii) at three sequential positions of the line during glide in Fig. 3G, demonstrating the evolution from almost pure screw dislocation to a serrated line and eventually to a more smoothly curved line. These observations suggest that the critical stress to move edge or mixed dislocations is not distinctly lower than that to move screw dislocations, which is not the case for conventional bcc metals at low homologous temperature. Rather, in conventional bcc metals, dislocations remain in a pure screw orientation as they migrate, because the nonscrew segments can glide away easily (*12*).

With increased stress from 812 to 938 MPa (Fig. 3, A and B), we observed highly variable motion among seemingly identical dislocations. Many dislocations [such as dislocation (i)] glide to the upper edge of the specimen and create long traces, whereas other dislocations [such as dislocations (ii) and (iii)] glide for only a short distance. Usually heterogeneous stress fields created by nearby defects would explain such variability, yet the defect environment in this region is not appreciably different. The different gliding behaviors of the dislocations in the same slip system suggest variations in the local lattice resistance for dislocation slip, originating at the atomic scale and not detectable at the current magnification.

Distribution of slip activities on high-order planes

The experimental observations of dislocations possessing largely nonscrew character on high-order slip planes are statistically robust over the course of loading and are homogeneously distributed across the entire single crystal (region that measured ~5 by 5 μm gauge) (Fig. 4), suggesting that successive source operation on a single plane leading to heterogeneous avalanche behavior is not favored. The single crystal yields at 812 MPa under tensile loading along the [001] crystal direction, which, upon considering the largest Schmid factor of m = 0.49 in the single crystal, agrees well with the measured bulk polycrystal compressive yield strength of 1100 MPa for MoNbTi (Fig. 1A). This comparison results in a Taylor factor of 2.76, which is in the range of 2.75 to 3.06 for

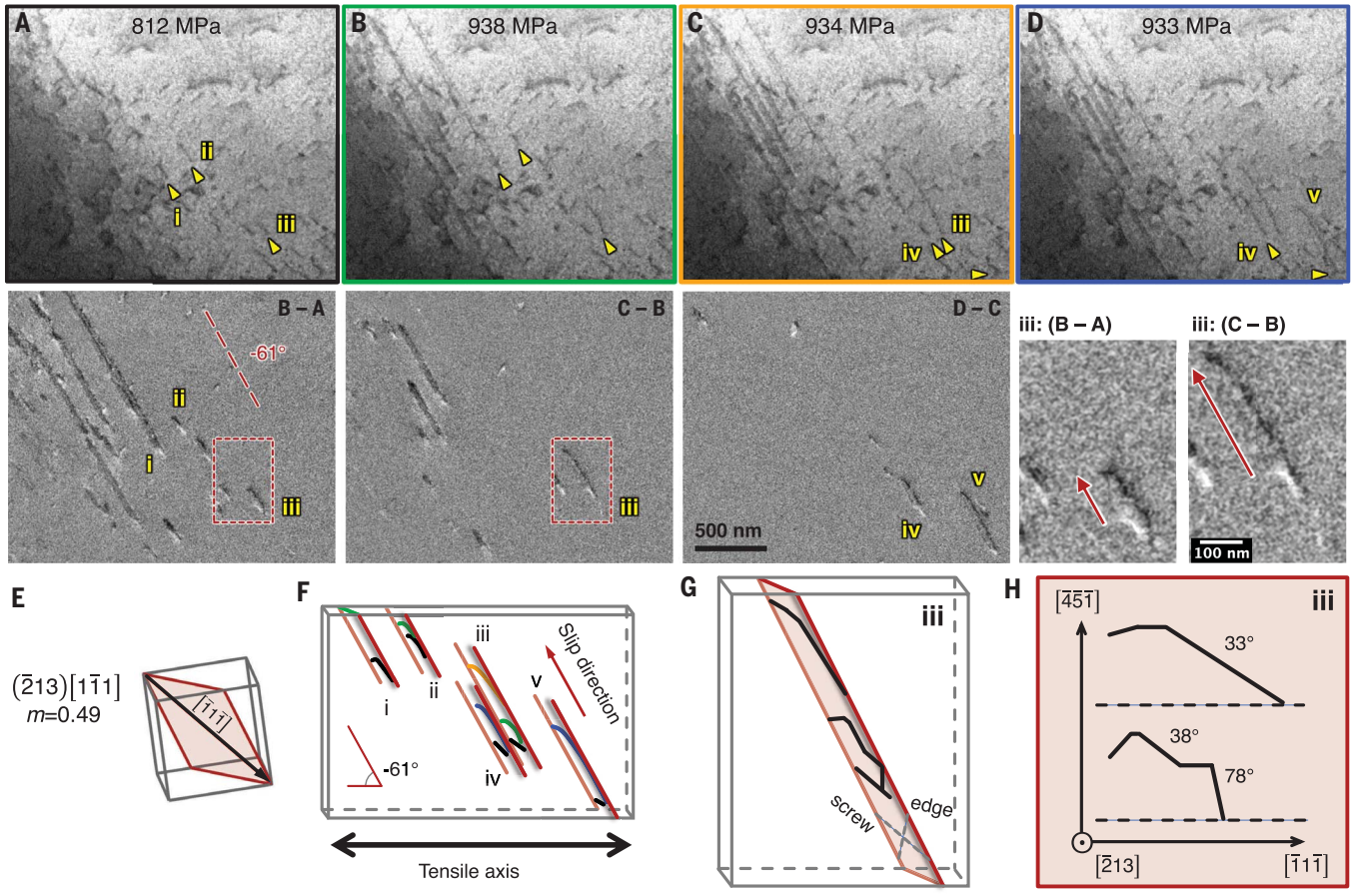

Fig. 3. Dynamic observation of dislocation bowing in the scanning electron microscope operating in transmission mode. (**A** and **B**) During loading. (**C** and **D**) At load-hold. The difference images between each of the two raw images are shown below. The parallel slip traces are measured to be at −61° from the horizontal (tension) direction. (**E**) Corresponding slip plane and Burgers vector shown from the same perspective as the images, including the Schmid factor *m*. The schematic isometric view in (**F**) shows the positions of selected dislocations colored by the respective images. The long and parallel lines in red are the slip traces. The evolution of dislocation (iii) is presented by the magnified difference images (B − A) and (C − B). The arrows indicate the slip direction from the original position (bright line) to the current position (dark line). These dislocation lines are reconstructed as thick black lines in (**G**), with pure edge and screw orientations indicated with dashed lines. (**H**) Line morphology of dislocation (iii) from the perspective of slip plane face-on. The horizontal and vertical axes are along the screw and edge orientations, respectively. The dislocation character angles for each segment are indicated.

typical bcc metals and close to 2.73 calculated for polycrystalline bcc metals deforming by pencil glide (*16*). Therefore, the activation of slip systems in the microtensile specimen is representative of that in a bulk polycrystalline material. The individually determined slip systems are active across the stress range without exhaustion (Fig. 4F). All of the measured slip traces are linked to high-order slip planes of {112}, {123}, and even {134} types.

To determine the origin of the glide-plane selection, we carried out a Schmid factor analysis for all recorded slip traces. Most of the active slip systems have high Schmid factors (0.42 to 0.49), with only a few systems having low Schmid factors (0.26 or 0.29) (table S5). We did not observe traces corresponding to the commonly considered {110} slip planes, even though some of these systems exhibit relatively high Schmid factors of 0.36, 0.40, or 0.45. The unexpected result of the selection of high-order slip planes with high Schmid factors could be rationalized by composite (effective) slip on various {110} planes through facile cross-slip. However, the absence of the traces of {110} slip systems with equally high Schmid factor (0.45) indicates that the slip resistances on the various high-order planes are comparable if not even lower, thereby favoring high-order planes. Additionally, our observations of mixed-character gliding dislocations would preclude the copious cross-slip of screw dislocations required to give rise to slip on effective (noncrystallographic) high-order planes according to the maximum RSS plane criterion (*17*). Considering the complex atomic distribution in MPEAs, our results motivate the hypothesis that the probability of moving dislocations on the observed high-order crystallographic slip planes is similar to or even higher than that on {110} planes, promoting slip selection on a widespread basis and uniformly over the crystal.

Slip resistance for dislocations in MoNbTi

In light of our experimental evidence for the nonscrew character of dislocations and the multiplicity of operative slip systems, we focused on the origin of the slip resistance for the edge and screw dislocations on different slip planes. Atomistic simulations reported the decreased ratio of the critical stress required to move screw and edge dislocations on {110} planes in NbTiZr, relative to conventional bcc metals and alloys, owing to the fluctuations of solute concentration (*10*) and the varying energy barrier for kink migration in a random solute environment of MPEAs (*18*). Our results suggest that examining only the common {110} slip planes in bcc MPEAs does not suffice in

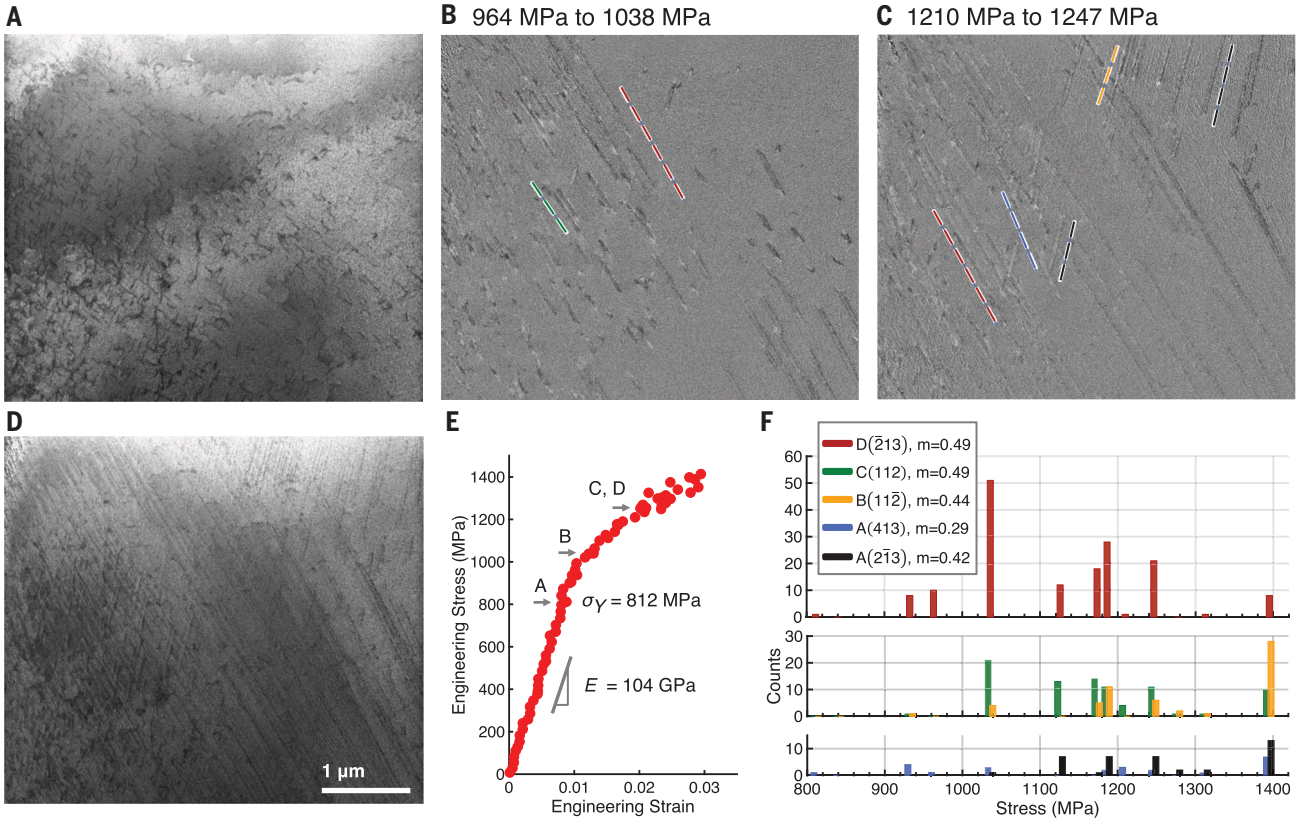

Fig. 4. The distribution of slip activities in the gauge region and across the tested stress values. (**A**) Initial microstructure of the gauge region. (**B** and **C**) Difference images showing the change in microstructure for the respective stress increments. (**D**) Deformed microstructure at 1247 MPa. (**E**) Engineering stress-strain data. (**F**) Distribution of the occurrence of slip activities at different stress values. The Burgers vectors are expressed according to the Schmid-Boas notation: $A = [\bar{1}11]$, $B = [111]$, $C = [11\bar{1}]$, and $D = [1\bar{1}1]$. The Schmid factors m are indicated.

accurately representing the three-dimensional fluctuation of chemistry. Reminiscent effects have been reported in NiAl hosting the B2 crystal structure (*19*), in which the Peierls stresses for screw and edge ⟨111⟩ dislocations were shown to be very similar on {112} planes, whereas they have a ratio of ~29 on {110} planes, and the Peierls stress for screw dislocations on {112} was slightly smaller than that on {110} planes.

We performed atomistic simulations to calculate the slip resistance in MoNbTi for screw and edge dislocations on {110}, {112}, and {123} planes. To reflect the influence of the local atomic environment and account for statistical fluctuations, calculations were performed by enforcing a short dislocation segment of length 3*b* to 4*b* (*b* is the magnitude of Burgers vector) to glide on the respective slip plane by one lattice periodicity, with multiple enumerations using different simulation cells. Each cell contains atoms that were randomly assigned to a bcc lattice on the basis of the equiatomic composition. The calculated slip resistance is akin to a Peierls stress in elemental and dilute alloys but, in MPEAs, is more accurately termed a local slip resistance (LSR), as it accounts for the periodic energy landscape of the crystal lattice as well as any local solute environment sampled by a dislocation as it moves in the globally random structure.

The computed LSR values have a broad distribution (Fig. 5) in contrast to the deterministic value in pure metals (the Peierls stress in a homogeneous lattice). The substantial variations result in dislocation glide of a probabilistic nature. Among the simulated dislocations, the lowest stress to move a dislocation (of edge character) can occur on either {110}, {112}, or {123} planes depending on the local atomic configuration. We observe that on the {112} planes, certain local atomic configurations can bear an LSR that is lower for screw dislocations than for edge dislocations. The dislocation slip asymmetry, owing either to twinning–anti-twinning asymmetry known for {112} planes (*17*) or to a shear in a positive or negative sense on other planes (Fig. 5B), also takes on a probabilistic nature. Slip in the anti-twinning direction is not always harder than in the twinning direction on {112} planes, as is the case for conventional bcc metals. Taken as a whole, the diminished distinctions between slip planes, dislocation characters, and even slip directions imply multiple pathways for dislocation slip, which is desirable for plastic formability and damage tolerance.

Discussion

Despite the decreased difference between the LSR to move screw and edge dislocations in MoNbTi, slip still occurs primarily by edge dislocations. What is distinctive to bcc MPEAs is that the straight screw dislocation could have a varying core structure along its line due to the local chemical fluctuations. As a result, the barrier for kink nucleation may be lowered, and kinks could even be preexisting (*10*, *20*, *21*). Once kinks are present on a screw dislocation on any of the {110}, {112}, and {123} planes, the edge character dislocation segments would glide on the slip plane that locally have the lowest resistance. On the basis of the series of simulations performed in MoNbTi, it appears that gliding on {123} planes is statistically the easiest (Fig. 5C), which agrees with the experimental observation that the active slip system at yield is $1/2[1\bar{1}1](\bar{2}13)$ (Fig. 3). Using the 812-MPa tensile yield stress of the experimental specimen and the Schmid factor of 0.49, we determined the RSS on the slip

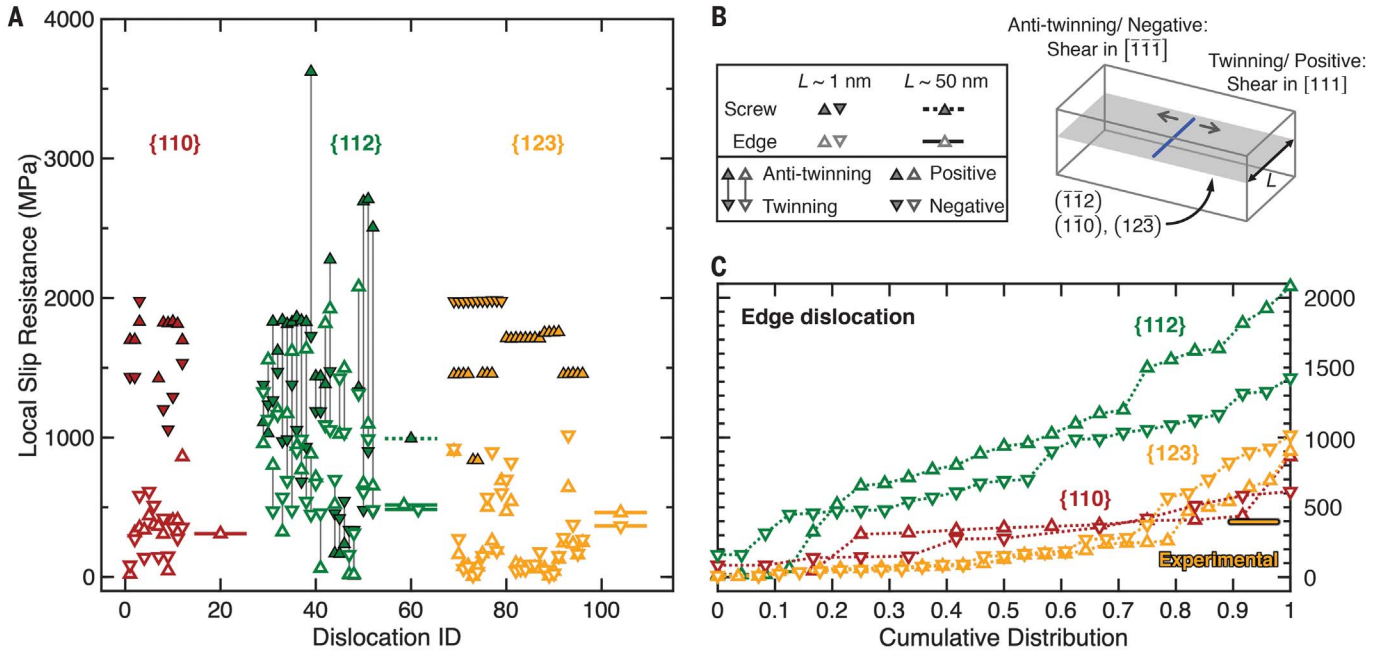

Fig. 5. Simulated LSR for screw and edge dislocations on {110}, {112}, and {123} planes in MoNbTi. (**A**) Simulations were performed respectively on screw (filled markers) and edge (open markers) character dislocations and on different types of planes (marker colors). Both short [length (L) ~ 1 nm] and long dislocations (L ~ 50 nm) were used to assess the effect of local chemistry. Each simulated dislocation is identified by an ID number. The same initial dislocation [shown as a thick blue line in the schematic in (**B**)] was moved to create shear in opposite directions to assess the slip sense asymmetry. If the shear created by dislocation glide is in the [111] direction, it is the twinning sense on $(\bar{1}\bar{1}2)$ plane and is denoted as the positive sense on $(1\bar{1}0)$ or $(12\bar{3})$ plane. If the shear is in the $[\bar{1}\bar{1}\bar{1}]$ direction, it is the anti-twinning sense and negative sense on the respective planes. Only the results of stably gliding dislocations are shown in the plot. (**C**) Cumulative distribution of the LSR values for edge dislocations is plotted. The experimentally determined resolved shear stress on the active slip system $1/2[\bar{1}\bar{1}1](\bar{2}13)$ (in Fig. 3) is shown as a thick horizontal line.

system to be 398 MPa. Compared with the computed LSRs, it is highly likely (at a probability of ~0.8) that the RSS is sufficient to activate edge dislocation motion on {123} planes. Together with the dominance of nonscrew segments on the observed dislocation lines, this quantitative comparison demonstrates that the high slip resistance of edge dislocations controls the yield stress in this alloy. On the other hand, rather than material softening by opting for the weakest link of gliding dislocations, the variation of the LSR in the same glide plane serves to suppress dislocation runaway and localized plastic flow, which is exhibited both as the increased tortuosity of the dislocation line and as multiple slip events in the crystal. Consistent with the statistical analysis of our experiments (Fig. 4), the traces of various slip systems are homogeneously distributed in the region on multiple high-order planes, and no localization is observed up to 600 MPa beyond yielding.

The probabilistic glide on {110}, {112}, {123}, and even {134} planes can contribute to retained strength at elevated temperatures, before the onset of diffusion-controlled dislocation glide/climb around 0.5 to 0.6 T_m (*22*). The efficacy of the solute-strengthening mechanism decreases with increasing temperature, because it is a thermally activated process by nature. The alternative strengthening mechanism of dipole dragging on screw dislocations depends weakly on a temperature below ~0.6 T_m, because it is based on the elastic interaction of dislocation segments. Frequent kink formation on different planes and the subsequent glide of the edge or mixed kink dislocation on different planes (*10*, *23*) are prerequisites for edge dipole formation, so the chances are greatly enhanced in MoNbTi by the activities on a large number of slip planes. The operation of dipole dragging strengthening, paired with the low extent of thermal elastic softening in the refractory bcc alloys (*24*), is likely responsible for the strength plateau in the intermediate temperature regime of MoNbTi (Fig. 1). However, the multiple operative slip planes may not be common in all bcc MPEAs, as evidenced by the diverse strength-temperature dependence (Fig. 1). This promotes the need to understand and even tailor the extent of dipole dragging and hence its contribution to hardening through a defect-aware alloy design strategy.

Our study reports clear, albeit unexpected, evidence for (i) a large fraction of nonscrew segments on the gliding dislocations in a bcc refractory MPEA at a low homologous temperature of 0.12 T_m, (ii) the importance of high-order slip planes in bcc MPEAs, and (iii) a probabilistic description of the slip resistance in random alloys. These results constitute the mechanistic basis that can explain the high strength and homogeneous plasticity of this alloy at a low homologous temperature, and they contribute to understanding its weak temperature dependence of strength. All three features are desirable for applications exposing materials to extreme temperatures yet are not simultaneously attainable in traditional refractory metals or alloys. These insights pave the way for theory-guided exploration of new alloys in the vast compositional space of MPEAs, as the multicharacter and multiplanar nature of dislocation slip could be employed as a mechanistic fingerprint for material screening. At a fundamental level, a probabilistic description of the traditional Peierls stress of dislocations owing to the fluctuating chemical landscape at the atomic scale should be brought to the forefront when designing new MPEAs.

REFERENCES AND NOTES

1. J. Yeh *et al.*, *Adv. Eng. Mater.* **6**, 299–303 (2004).
2. B. Cantor, I. Chang, P. Knight, A. Vincent, *Mater. Sci. Eng. A* **375-377**, 213–218 (2004).
3. D. Miracle, O. Senkov, *Acta Mater.* **122**, 448–511 (2017).
4. B. Gludovatz *et al.*, *Science* **345**, 1153–1158 (2014).
5. B. Gludovatz *et al.*, *Nat. Commun.* **7**, 10602 (2016).
6. B. Butler *et al.*, *Int. J. Refract. Met. Hard Mater.* **75**, 248–261 (2018).
7. O. Senkov, D. Miracle, K. Chaput, J.-P. Couzinie,*J. Mater. Res.* **33**, 3092–3128 (2018).

8. O. Senkov, G. Wilks, D. Miracle, C. Chuang, P. Liaw, *Intermetallics* **18**, 1758–1765 (2010).
9. O. Senkov, G. Wilks, J. Scott, D. Miracle, *Intermetallics* **19**, 698–706 (2011).
10. S. Rao *et al*., *Acta Mater.* **168**, 222–236 (2019).
11. F. Maresca, W. Curtin, *Acta Mater.* **182**, 235–249 (2020).
12. B. Sestak, A. Seeger, *Z. Metallk.* **69**, 195–202 (1978).
13. L. Lilensten *et al*., *Acta Mater.* **142**, 131–141 (2018).
14. Materials and methods are available as supplementary materials.
15. M. Butt, *Philos. Mag.* **87**, 3595–3614 (2007).
16. J. Rosenberg, H. Piehler, *Metall. Trans.* **2**, 257–259 (1971).
17. C. Weinberger, B. Boyce, C. Battaile, *Int. Mater. Rev.* **58**, 296–314 (2013).
18. F. Maresca, W. Curtin, *Acta Mater.* **182**, 144–162 (2020).
19. P. Gumbsch, R. Schroll, *Intermetallics* **7**, 447–454 (1999).
20. H. Suzuki, "Solid solution hardening in body-centered cubic alloys" in vol. 4 of *Dislocations in Solids* (1980), 191–217.
21. S. Rao *et al*., *Acta Mater.* **125**, 311–320 (2017).
22. O. Senkov, S. Gorsse, D. Miracle, *Acta Mater.* **175**, 394–405 (2019).
23. D. Caillard, *Acta Mater.* **61**, 2808–2827 (2013).
24. G. Laplanche, P. Gadaud, L. Perriere, I. Guillot, J. Couzinie, *J. Alloys Compd.* **799**, 538–545 (2019).
25. J. P. Couzinié, O. N. Senkov, D. B. Miracle, G. Dirras, *Data Brief* **21**, 1622–1641 (2018).
26. J. Bechtold, *Acta Metall.* **3**, 249–254 (1955).
27. F. Schmidt, H. Ogden, "The engineering properties of tungsten and tungsten alloys" (DMIC Report 191, Battelle Memorial Institute, 1963).
28. ATI Wah Chang Nb/Nb Alloy C-103. MatWeb (2020); http://www.matweb.com/search/DataSheet.aspx?MatGUID=ed50a3a07706450590669cedc7784150.
29. P/M Molybdenum TZM (Mo-0.5Ti-0.1Zr; Mo Alloy 364), Stress Relieved. MatWeb (2020); http://www.matweb.com/search/DataSheet.aspx?MatGUID=1868b5a70b8240999ccc55468cc90c9e.

ACKNOWLEDGMENTS

We thank C. Woodward and S. Rao at the Air Force Research Laboratory for fruitful discussions and for providing detailed comments on the manuscript, and P. Callahan at the U. S. Naval Research Laboratory for assistance with atom-probe specimen preparation. We also thank K. Dang for helpful discussions on the periodic array of dislocations model. **Funding:** This work was funded by the Office of Naval Research, Basic Research Challenge Program (grant no. N00014-18-1-2392). The work of S.X. was supported in part by the Elings Prize Fellowship in Science offered by the California NanoSystems Institute (CNSI) on the UC Santa Barbara campus. The work of K.E.K. was supported in part by a Department of Defense Basic Research Office Laboratory University Collaboration Initiative (LUCI) fellowship. The work of O.N.S. was supported through the United States Air Force on-site contract (FA8650-15-D-5230). The experimental work made use of the MRL Shared Experimental Facilities at UC Santa Barbara supported by the Materials Research Science and Engineering Center (MRSEC) Program of the National Science Foundation (NSF) (award no. DMR 1720256), a member of the NSF-funded Materials Research Facilities Network (www.mrfn.org). Use was made of computational facilities purchased with funds from the NSF (CNS-1725797) and administered by the Center for Scientific Computing (CSC). The CSC is supported by the CNSI and the MRSEC. This work used the Extreme Science and Engineering Discovery Environment (XSEDE), which is supported by NSF (grant no. ACI-1053575). **Author contributions:** O.N.S. synthesized the material and conducted bulk mechanical tests. L.H.M. performed chemical analyses. K.E.K. performed atom probe tomography experiment and analysis. G.H.B. performed nanoindentations. F.W. and P.F.R. performed ex situ TEM analyses of the dislocations after nanoindentation. F.W., G.H.B., and J.-C.S prepared samples and performed in situ tests in scanning electron microscopy. F.W. and J.S. analyzed the in situ test data. S.X. and Y.S. performed the atomistic simulations. F.W., O.N.S., I.J.B., T.M.P., and D.S.G. jointly designed and interpreted the study and prepared the manuscript. All authors contributed to the discussion and revision of the manuscript. **Competing interests:** The authors declare no competing interests. **Data and materials availability:** All data are available in the manuscript or the supplementary materials.

SUPPLEMENTARY MATERIALS

science.sciencemag.org/content/370/6512/95/suppl/DC1
Materials and Methods
Supplementary Text
Figs. S1 to S6
Tables S1 to S8
References (*30*–*53*)

27 November 2019; accepted 2 July 2020
10.1126/science.aba3722

Multiplicity of dislocation pathways in a refractory multiprincipal element alloy

Fulin Wang, Glenn H. Balbus, Shuozhi Xu, Yanqing Su, Jungho Shin, Paul F. Rottmann, Keith E. Knipling, Jean-Charles Stinville, Leah H. Mills, Oleg N. Senkov, Irene J. Beyerlein, Tresa M. Pollock and Daniel S. Gianola

Science **370** (6512), 95-101.
DOI: 10.1126/science.aba3722

Pathways for ductility

Alloys containing multiple elements can be very strong but often suffer from poor ductility. F. Wang *et al.* found that different mechanisms accommodated plasticity in a molybdenum-niobium-titanium multiprincipal element alloy (see the Perspective by Cairney). Instead of so-called "screw" dislocations, deformation is accommodated by multiple pathways that include "edge" dislocations and activation of crystallographic slip planes. These results offer a design paradigm for developing new high-strength alloys.

Science, this issue p. 95; see also p. 37